Controlling the generation of THz radiation from metallic films using periodic microstructure

D. K. Polyushkin[1,2], E. Hendry[1] and W. L. Barnes[1]

[1] School of Physics and Astronomy, University of Exeter, Stocker Road, Exeter EX4 4QL, UK

[2] Institute of Photonics, Vienna University of Technology, Gusshausstrasse 27-29, 1040 Vienna, Austria

Abstract. We report on THz frequency generation via irradiation of microstructured semicontinuous silver films by femtosecond laser pulses. By patterning the film so as to produce an array of microstrips, we show that one can use periodic microstructure to control the way nanostructured metal films produce THz radiation when illuminated by femtosecond infrared laser pulses. A simple analytical model based on the field distribution arising from an array of THz dipole emitters is used to assess the experimental data, allowing us to explain some of the main features of the generated THz radiation patterns, including the strongly resonant features of the emission spectrum.

I. Introduction

A THz gap [1] has been highlighted in the electromagnetic spectrum, due to a lack of traditional sources and detectors in this frequency region. This situation has begun to change in recent years, with the development of free electron lasers [1], [2], quantum cascade lasers [3], and table top spectrometers based on ultrafast laser pulses [4]. The production of THz radiation via ultrafast laser irradiation of a number of materials has been shown to occur via various mechanisms: optical rectification in nonlinear dielectric materials [5], photoexcited plasmas in gases [6], demagnetisation in ferromagnets [7] and via the surface field emission and photo-Dember effects in semiconductors [8], [9], amongst other mechanisms.

In recent years a number of experiments have been undertaken to explore THz emission arising from illumination of metallic interfaces with infrared pulses of light. The first experiments on THz generation by femtosecond laser pulses from optically thin metal surfaces were published in 2004 [10]. Since then different metallic materials and structures were used to generate THz radiation: nanostructured silver and gold films [11], [12]; semicontinuous metal films [13], [14]; and nanoparticles [12], [14]. In all these experiments the resulting spectrum of the THz radiation has quite a broad spectrum with an intensity maximum at ca. 0.5 THz, a consequence of the chosen parameters of the incident light, mainly the incident laser pulse width. While two distinct mechanisms have been proposed to explain the observed generation of THz radiation in different intensity regimes (optical rectification on thin metal films [10], [12], [13], [15]–[17] and radiation produced by accelerated charges due to the liberation and subsequent acceleration of electrons from the metal by strong electric fields in proximity to metal surfaces [11], [12], [14]), both mechanisms invoke a dipole moment for the generation that is oriented

along the surface normal. This dipole orientation results in no THz radiation being generated when films are illuminated at normal incidence, THz emission gradually increasing as the angle of illumination is increased. This situation results in relatively low intensities of generated THz radiation, and is in many ways analogous to THz generation via the photo-Dember effect, where greater emission of THz radiation for normal incidence excitation can be achieved by applying a magnetic field perpendicular to the plane of incidence [18], resulting in realignment of the THz dipole moment.

To illustrate this issue further, consider THz radiation produced as a result of electron ejection and acceleration from a metal nanoparticle, as indicated in Figure 1a. For illumination under normal incidence the only net current produced by the ejected electrons is along the surface normal, currents produced in the plane of the surface cancel out. The net current perpendicular to the surface in turn produces THz radiation in the plane of the surface, as indicated in Figure 1a. For samples comprising a large number of nanoparticles on a surface, Figure 1b, the THz radiation produced by different particles will vary in phase according to the distance between the particles. As a result, for samples whose dimensions are bigger than the THz wavelength (~0.1 mm) the net production of THz will be zero owing to destructive interference.

In this work we explore THz frequency generation via irradiation of microstructured semicontinuous silver films by femtosecond laser pulses. The use of periodic microstructuring of the surface, Figure 1c, overcomes the problem of destructive interference in much the same way that period-poling does for optical parametric generation [19]. As a result the directional and frequency dependence of the emitted THz radiation can now be controlled through the sample geometry. In particular THz emission can now be produced for illumination close to normal incidence. A simple analytical model based on calculating radiation interference from dipole emitters in the far-field is used to describe the experimental data, allowing us to explain some of the main features of the generated radiation from both structured and non-structured samples.

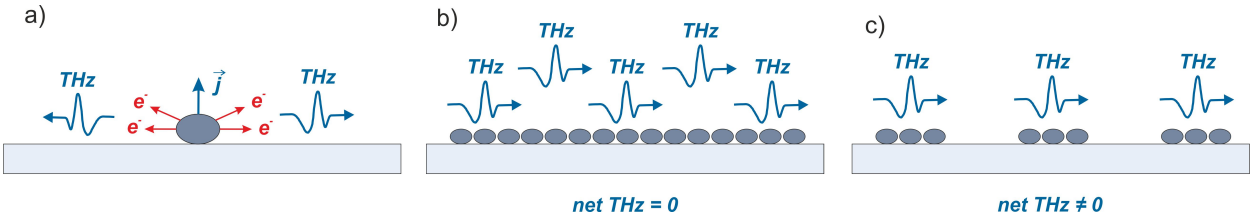

Figure 1. Sketches showing THz generation. (a) The net current produced by the ejected electrons is normal to the substrate, the THz is thus radiated predominantly along the surface direction. (b) For particles uniformly distributed on the surface the THz produced by all the particles adds up destructively. (c) Microstructuring of the area of the sample covered by particles leads to quasi-phase-matching of the THz generation and results in non-zero THz field in the far-field.

II. Sample preparation and the experimental setup

Two samples were prepared for the experiments. A uniform sample is fabricated by evaporation of 15 nm of silver under vacuum (below 10^{-5} mbar) at a deposition rate of 1 Å/s onto cleaned glass substrates (microscope cover slips with the thickness of ~0.1mm). It was shown previously [13], [14] that silver films with thicknesses less than 20 nm can generate THz radiation by illuminating them with

femtosecond laser pulses. The structured sample was fabricated in the same way, but the evaporation of metal took place through a mask comprising rectangular apertures of width 300 µm separated by gaps of width 300 µm, thus giving an array of electrically disconnected bars with 1:1 mark-to-space ratio, and period of 600 µm (Figure 6a). The same thickness of silver was used as for the uniform sample.

For THz generation and detection we use 100 fs laser pulses with a central wavelength of 800 nm from an amplified Ti:sapphire laser in standard THz time-domain setup [14]. For generation of THz radiation we use the samples under investigation and for the detection 1 mm thick ZnTe 110-oriented electro-optical crystal. The laser beam was split into two beams, one for THz generation and the other for detection of the generated THz radiation. The pulses were focused to a spot size of ~ 1.5 mm giving an incident intensity of order of 10 GW/cm^2, the intensity we used for all the experiments reported here. While we have not directly measured the absolute THz pulse energy, by estimating the THz field strength and spot size we can make a rough estimate of ca. 1 - 10 fJ for an incident excitation fluence of 10 GW/cm^2. This is comparable to the pulse energies generated in the reports [16], [17].

The sampling technique allows us to measure the transient THz field. Recorded time-domain field is used to retrieve the radiation spectrum by means of Fourier transform. Representative spectra and time-domain signal are shown in Figure 5b. To reduce the absorption of THz radiation by water vapours the setup is placed in closed box filled with dry air. It should be also noted that the generation intensity from the bare substrates were below the noise floor of the detection setup, while the strongest signals obtained from the sample under investigation are above 2 orders of magnitude higher than the noise level.

III. Analytical model

We begin by introducing a simple model which describes the emission pattern of a phase coupled array of dipoles at an interface. For the sake of simplicity, we consider a linear array of dipole emitters continuously distributed along the line (Figure 2).

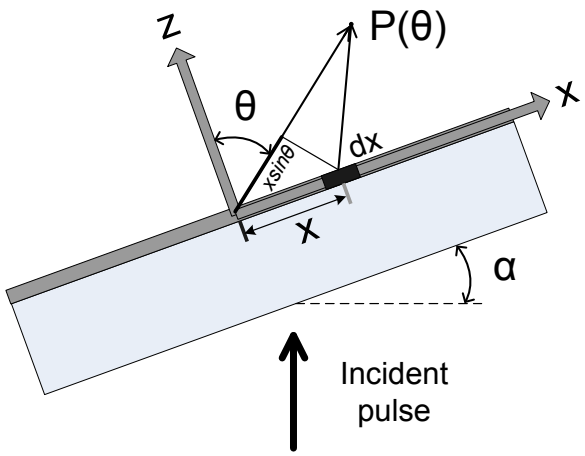

Figure 2. Schematic representation of the modelled sample with uniform distribution of emitters.

The resulting field distribution in the far-field $E(\theta)$ of an array of dipoles is a product of the *radiation pattern* (RP) of a single dipole $\Phi(\theta)$ and the *directivity factor* of the system of emitters $F(\theta)$, the interference of the radiation from all the emitters, $E(\theta)=\Phi(\theta)F(\theta)$. The second term can be expressed as follows

$$F(\theta)=\int_{-L/2}^{L/2} A(x)\exp(ikx\sin\theta)dx, \qquad (1)$$

here $x\sin\theta$ is the difference in the beam paths of the radiation emitted at the origin and at the coordinate x, $A(x)$ the amplitude and phase field distribution along the illumination spot with the size L and $k = 2\pi/\lambda_{THz}$ the wavenumber of the THz radiation. To simplify the model we assume a uniform distribution of incident light intensity along the illumination spot. While the amplitude of the excitation intensity is uniform, the phase φ has linear dependence on the coordinate $\varphi(x)=-kx\sin\alpha$, as defined in Figure 2. Thus $A(x)$ can be expressed as

$$A(x)=A_0\exp(-ikx\sin\alpha), \qquad (2)$$

where A_0 is linear density of the emitted field strength. Using expression (2), the relation (1) can be rewritten in the form

$$F(\theta)=\int_{-L/2}^{L/2} A_0\exp(ikx(\sin\theta-\sin\alpha))dx = A_0L\frac{\sin\psi}{\psi}, \qquad (3)$$

where $\psi(\theta)=\frac{1}{2}kL(\sin\theta-\sin\alpha)$. The function $\sin\psi/\psi$ is maximal and equals 1 at $\psi = 0$, i.e. when $\sin\theta=\sin\alpha \Rightarrow \theta=\alpha$. This means that the directivity factor is maximal in *in-line detection*, i.e. when the THz detector is placed in the line of incident excitation beam. Another feature of the in-line detection is that the directivity factor does not depend on the wavelength of the generated THz radiation. In Figure 3 the function (3) is plotted for 3 different wavelengths 0.33 THz, 0.5 THz and 1 THz versus the detection angles with the angle of incidence $\alpha = 0$. From the Figure 3 it can be seen that only for in-line detection does the radiation in the far-field from all the dipoles add up in phase. At any other detection angles frequency selection due to interference of the emitters occurs.

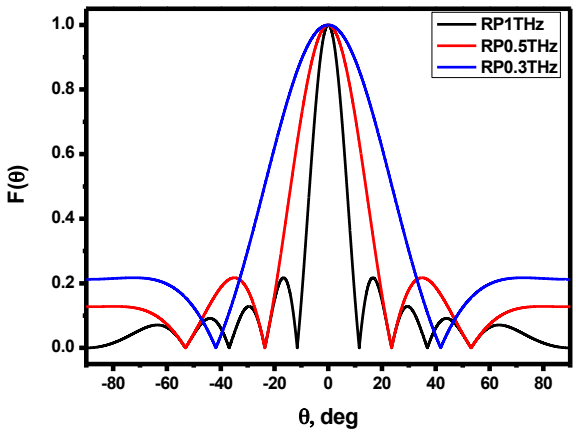

Figure 3. Directivity factor as a function of the detection angle θ with angle of incidence $\alpha = 0$. Blue, red and black lines correspond to the frequencies 0.33 THz, 0.5 THz, 1 THz, respectively.

The model described above deals only with p-polarized THz radiation, i.e. emitted in the plane of incidence. Only for this polarization is there an excitation phase difference depending on the angle of incidence and thus in phase sum up of the radiation in the far-field for the in-line detection. For dipoles distributed along the rotation axis in plane of the sample there is no excitation phase difference and thus the radiation from these dipoles destructively interfere in the far-field. This corresponds to the case when α always equals 0 in relation (3), which leads to polarization of THz radiation in plane of incidence for any incident light polarization states. We determine in experiment (Figure 4) that THz radiation from silver films is indeed highly polarized in the plane of incidence, with the orthogonal polarization intensity three orders of magnitude weaker.

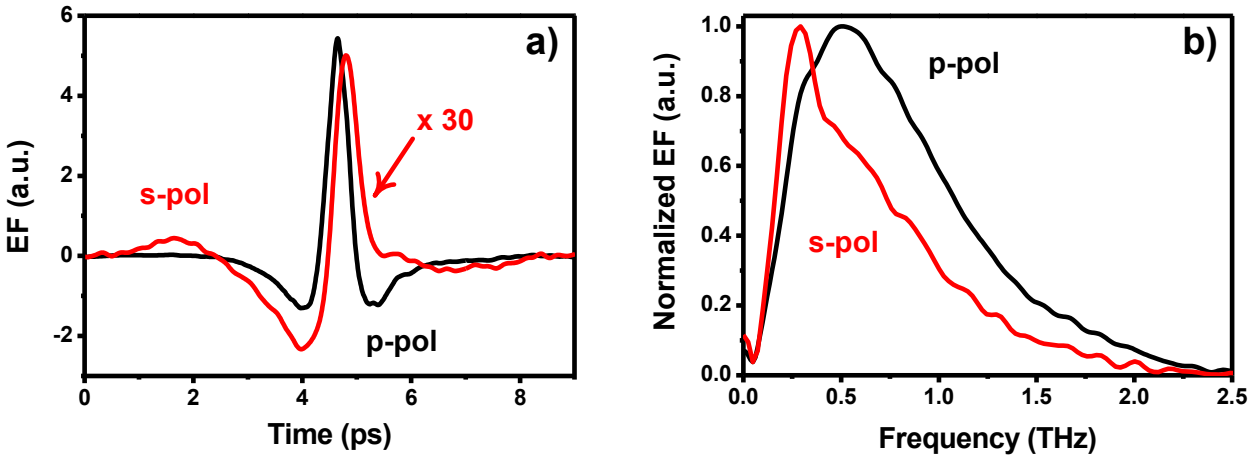

Figure 4. Time-domain signals (a) and pulse spectra (b) from semicontinuous silver films measured for two polarizations, p (black) and s (red). S-polarized signal in (a) is multiplied by a factor of 30.

Let us consider the radiation pattern of Hertzian dipole emitters with dipole moment oriented perpendicular to the surface. The density of the radiated intensity generated in small solid angle $d\sigma$ is expressed by the formula

$$d\Phi^2(\theta) \sim N\ddot{d}^2 \sin^2\theta d\sigma, \qquad (4)$$

where d is the dipole moment of the emitter and N the density of the emitters. Differential of solid angle σ can be expressed as follows $d\sigma = 2\pi \sin\theta d\theta$. Taking into account the last expression and the fact that the collection angles of the parabolic mirrors in the setup are small, expression (4) can be then rewritten as

$$\Phi^2(\theta) \sim N\ddot{d}^2 \sin^3\theta \qquad (5)$$

The product of the density of dipole emitters and the second order time derivative of the dipole moment is proportional to the intensity of THz radiation, which in turn is proportional to the incident intensity to the power n, since $N\ddot{d}^2 \sim I_{THz} \sim I_{opt}^n$ [14]. Here I_{opt} is an intensity of the incident light and n the order of the THz generation process. Since incident light intensity on the surface of the sample is inversely proportional to the spot size, then $I_{opt}(\alpha) = I_0 S_0 / S(\alpha) = I_0 S_0 / (S_0 / \cos\alpha) = I_0 \cos\alpha$, where I_0 is an intensity of the incident light in the beam. Combining the last two expressions and assuming in-line detection, i.e. $\theta = \alpha$, the angle dependence of the radiation pattern is then given by

$$\Phi^2(\alpha) \sim I_0^n \sin^3\alpha \cos^n\alpha \qquad (6)$$

The equations obtained above are valid to describe any emission given by an induced dipole moment orientated along the surface normal, and can therefore describe both proposed processes, optical rectification on thin metal films [10], [13], [15]–[17] and radiation of accelerated charges due to liberating and subsequent accelerating of electrons from the metal by high electric field in proximity to metal surfaces [11], [14]. In relation to the generation mechanism, we have discussed different possible mechanisms in an earlier paper [12]. Indeed, the measurements in that paper indicate at least two different mechanisms of THz generation from metal structures under femtosecond laser pulse illumination: optical rectification and acceleration of emitted electrons. These two mechanism may act at the same time and differ only in the order of the dependence of the THz fluence on the incident illumination intensity. Depending on the type of the structure and on the intensity of the incident light one of the mechanisms may take over another. However, because of the high order intensity dependence for semicontinuous metal film in this range of pump pulse intensities [14], we conclude that the generation mechanism which invokes the emission of electrons is dominant.

For the considered sample geometry, THz radiation from dipoles having their moments along the surface cancels in far-field due to symmetry, see Figure 1a. This means that very little THz radiation is generated when films are illuminated at normal incidence, although emission gradually increases on increasing the angle of illumination.

IV. Experimental results

a. In-line detection

The predicted above effects can be demonstrated experimentally by measuring the angle dependence of THz intensity with the detector placed in the line with the incident beam. For simplicity we refer to this detection setup as the *in-line detection*. The results are shown in Figure 5a together with the fit based on the formula (6) with two different values of the nonlinearity parameter n equals 3 and 5.

These numbers represent the range in nonlinearity found for THz intensity dependences on incident optical intensities for low energy pulses [14].

From the Figure 5a it follows that there is an optimal angle for THz generation ~50 degrees, with low intensities generated at both normal and grazing incidence. The scan of THz intensity vs angle of incidence for a range of incident angles from -80 to 80 degrees (Figure 5a inset) reveals inversion of the generated field phase without change of the amplitude on reversing the angle of incidence. The absence of the strong intensity radiation at normal incidence illumination suggests that the radiation from the dipoles with a moment parallel to the surface is negligible. Indeed, the THz intensity at $\alpha = 0$ is more than 3 orders of magnitude weaker than the maximum intensity at $\alpha = 50^{\circ}$.

For the in-line detection, the radiation from all the dipoles will add in phase (see (3)) and thus the directivity factor $F(\theta)$ does not depend on the angles θ and α. Since the shape of the radiation pattern $\Phi(\theta)$ does not depend on the angle of incidence either, it is expected that the spectra of radiation will not depend on angle of incidence. This is supported by experiment, it can be seen from the Figure 5b that the measured THz radiation spectra are simply scale in amplitude as a function of the angle of incidence without strong change in shape.

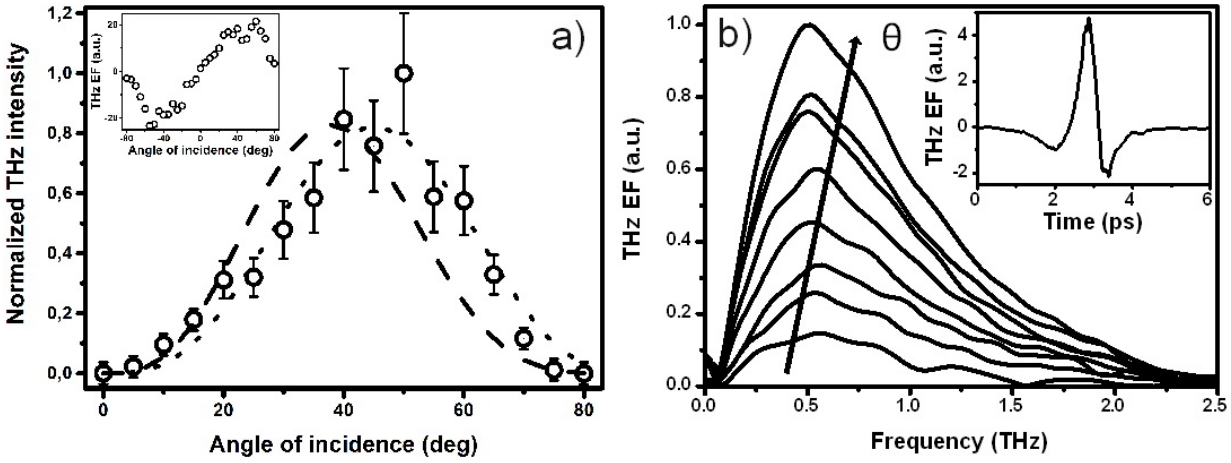

Figure 5. a) Intensity of THz radiation as a function of angle of incidence for non-structured sample. Lines represent the fitting of the experimental data with different parameter n: for dotted line $n = 3$ and for dashed $n = 5$. Inset: THz electric field strength in the range of incident angles from -80 to 80 degrees. b) THz spectra from uniform semicontinuous silver film obtained in in-line detection for angles of incidence ranging from 5 to 40 degrees with 5 degrees step. Inset: time-domain signal for angle of incidence 40 degrees.

b. Perpendicular detection

Let us now consider the properties of the radiation detected in the direction of $\theta = 90$ degrees for normal incidence excitation. For simplicity we call this detection setup as *perpendicular detection*. The emission efficiency for a single dipole is greatest in this direction. However, in the limit case with the excitation spot size L significantly greater than the THz wavelengths, the radiation in the direction $\theta = 90$ from each dipole cancels out in the far-field due to destructive interference. In Figure 6b we present measurements of the THz spectrum generated in the direction $\theta = 90$ degrees when the

sample is illuminated at normal incidence, the THz intensity is rather low in this geometry. Moreover, the spectrum exhibits a clear oscillatory pattern as a function of frequency. This behaviour occurs due to the finite size of the excitation beam on the sample, and thus the generated frequencies depend on the spot size L. The directivity factor can be obtained from the relation (3) using values of $\theta = 90^\circ$ and $\alpha = 0^\circ$, resulting in $\psi = \frac{1}{2}kL = \pi L/\lambda_{THz}$. To calculate the emitted spectrum, we multiply the directivity factor by the broad spectrum of a single emitter extracted from the results of THz generation from uniform semicontinuous silver film (Figure 5b). As can be seen from Figure 6b there is a clear correlation between the predicted spectrum from this model (dotted line) and the measured result (solid line). We have some disagreement in the spectral positions of peaks and troughs, especially for frequencies beyond 0.6 THz, which can be expected for such a simple model. The noise in the experimental data is due to strong suppression of the THz signal in the far-field as a result of destructive interference of the radiation from different sources across the illumination spot. Nevertheless, the origin of the features in the spectrum is clear by considering the dimensionless parameter L/λ_{THz}. For large spot sizes or short wavelength the effect of the destructive interference will be greater than for small spot sizes or long wavelengths. This effect limits the frequency bands of the spectrum, and results in rather weak emission amplitudes and a very noisy spectrum.

To overcome this limitation one can engineer the sample to allow radiation of certain wavelengths to constructively interfere in the perpendicular direction (or, in principal, any emission direction). This allows us to generate *constructive* THz emission in a direction *perpendicular* to the emission dipole, which will *optimize the emission intensity*. The simplest way to do this is remove dipoles which give a negative phase contribution in the far-field. This is done by structuring the material in strips, as depicted in Figure 6a. For wavelengths equal to the period of the strip array, constructive interference of dipole emission is now possible. It is important to note that this approach works only for a specific wavelengths defined by the design of the structure, i.e. the structure controls the generated frequencies. To demonstrate this idea we fabricated the structured sample shown in Figure 6a and measured the THz radiation generated in the direction $\theta = 90$ degrees. The results obtained for this sample are shown in Figure 6c. We now see a pronounced emission peak at ~0.5 THz as expected from the structure spatial period.

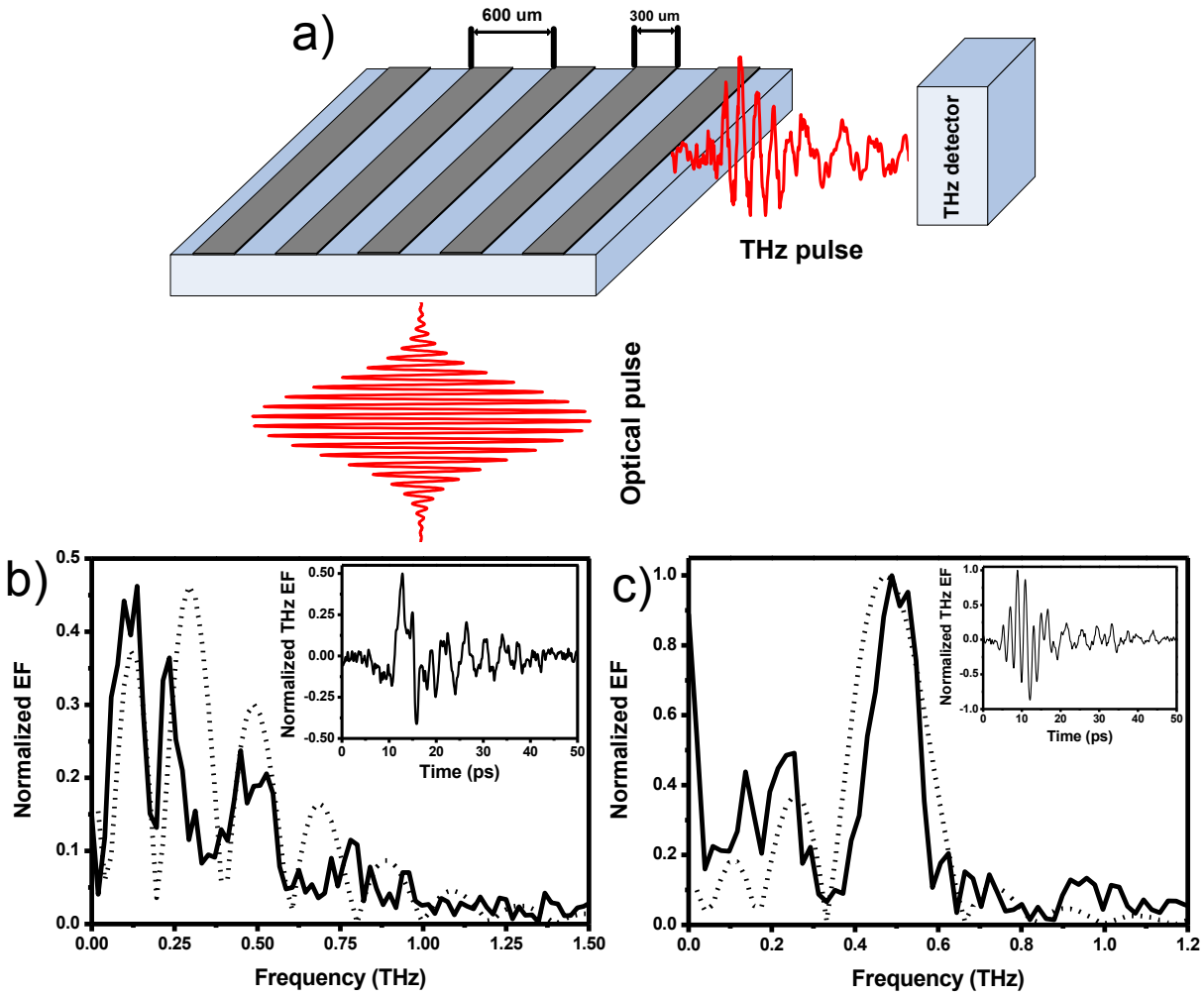

Figure 6. a) The sketch of the structured silver film. Comparison of the experimental (solid line) and theoretical (dot line) THz spectra from b) non-structured sample and c) structured sample in perpendicular detection. Insets in b) and c): time-domain signals from the corresponding samples. The data in b) show relative EF strength in respect to the normalised signal in c).

One can gain an insight into this behaviour by considering the directivity parameter for a structured sample, described as a set of the uniform strips with thickness $b = 300\ \mu m$ and period $d = 600\ \mu m$ (Figure 6a). The directivity factor for the sample then can be expressed as a geometric progression

$$\sum_{n=1}^{N} I\exp\left(ik(n-1)d\left(\sin\theta-\sin\alpha\right)\right)=I\sum_{n=1}^{N}q^{n-1}=I\frac{q^N-1}{q-1}, \qquad (7)$$

where $I = I_0 L\sin(\psi)/\psi$ with $\psi = \tfrac{1}{2}kb(\sin\theta-\sin\alpha)$ is the radiation from a single strip and $q=\exp\left(ikd\left(\sin\theta-\sin\alpha\right)\right)$. The following transformation can be applied to the expression (7) with a designation $\xi = kd(\sin\theta-\sin\alpha)$

$$\frac{e^{i\xi N}-1}{e^{i\xi}-1}=\frac{e^{i\xi N/2}\left(e^{i\xi n/2}-e^{-i\xi n/2}\right)}{e^{i\xi/2}\left(e^{i\xi/2}-e^{-i\xi/2}\right)}=e^{i\xi(N-1)/2}\frac{\sin\left(\xi N/2\right)}{\sin\left(\xi/2\right)} \quad (8)$$

Finally, combining the results from expressions (7) and (8), for amplitude of the directivity factor the following expression is obtained

$$F(\theta)\sim\left|\frac{\sin(\psi)}{\psi}\frac{\sin(N\chi)}{\sin(\chi)}\right|, \quad (9)$$

where $\chi=\frac{1}{2}kd\left(\sin\theta-\sin\alpha\right)$ and N is the number of illuminated strips which in our case equals 3.

The theoretical results from the expression (9) for normal incidence illumination ($\alpha = 0^o$) and perpendicular detection ($\theta = 90^o$) are compared with the experimental results in Figure 6c. Experiment and theory agree well, particularly for the dominant peak emission at ~0.5 THz. At this peak frequency, for the same excitation fluence, the radiation intensity emitted by the microstructured sample is 25 times greater than from the uniform film, despite having an active area which is 50% smaller.

To conclude, we fabricated and investigated microstructured semicontinuous silver films designed to generate resonant THz frequencies under illumination by a femtosecond pulse, with resonant frequencies defined by the sample geometry. By patterning the film in an array of microstrips, we showed that one can generate *constructive* THz emission in a direction *perpendicular* to the emission dipole. This results in the microstructured film emitting a significantly greater THz radiation intensity when compared to a uniform film. To understand our results we developed a simple analytical model based on the field distribution for an array of THz dipole emitters. The model describes some main features of the generated THz radiation, including the angle dependences of emitted radiation patterns and the resonant features of the emission spectrum.

References

[1] G. P. Williams, "Filling the THz gap—high power sources and applications," *Reports Prog. Phys.*, vol. 69, no. 2, pp. 301–326, Feb. 2006.

[2] G. L. Carr, M. C. Martin, W. R. McKinney, K. Jordan, G. R. Neil, and G. P. Williams, "High-power terahertz radiation from relativistic electrons," *Nature*, vol. 420, no. 6912, pp. 153–6, Nov. 2002.

[3] R. Köhler, A. Tredicucci, and F. Beltram, "Terahertz semiconductor-heterostructure laser," *Nature*, vol. 417, no. 6885, pp. 156–9, May 2002.

[4] K. Sakai, *Terahertz Optoelectronics*, vol. 97. Berlin: Springer, 2005, p. 350.

[5] J. Shan, A. Nahata, and T. F. Heinz, "Terahertz Time-Domain Spectroscopy Based on Nonlinear Optics," *J. Nonlinear Opt. Phys. Mater.*, vol. 11, no. 01, pp. 31–48, Mar. 2002.

[6] Y. Chen, M. Yamaguchi, M. Wang, and X.-C. Zhang, "Terahertz pulse generation from noble gases," *Appl. Phys. Lett.*, vol. 91, no. 25, p. 251116, 2007.

[7] E. Beaurepaire, G. M. Turner, S. M. Harrel, M. C. Beard, J.-Y. Bigot, and C. A. Schmuttenmaer, "Coherent terahertz emission from ferromagnetic films excited by femtosecond laser pulses," *Appl. Phys. Lett.*, vol. 84, no. 18, p. 3465, 2004.

[8] A. Reklaitis, "Crossover between surface field and photo-Dember effect induced terahertz emission," *J. Appl. Phys.*, vol. 109, no. 8, p. 083108, 2011.

[9] M. B. Johnston, D. M. Whittaker, A. Corchia, A. G. Davies, and E. H. Linfield, "Simulation of terahertz generation at semiconductor surfaces," *Phys. Rev. B*, vol. 65, no. 16, p. 165301, Mar. 2002.

[10] F. Kadlec, P. Kuzel, and J. L. Coutaz, "Optical rectification at metal surfaces," *Opt. Lett.*, vol. 29, no. 22, pp. 2674–2676, 2004.

[11] G. H. Welsh and K. Wynne, "Generation of ultrafast terahertz radiation pulses on metallic nanostructured surfaces," *Opt. Express*, vol. 17, no. 4, pp. 2470–2480, 2009.

[12] D. K. Polyushkin, I. Márton, P. Rácz, P. Dombi, E. Hendry, and W. L. Barnes, "Mechanisms of THz generation from silver nanoparticle and nanohole arrays illuminated by 100 fs pulses of infrared light," *Phys. Rev. B*, vol. 89, pp. 125426:1–7, 2014.

[13] G. Ramakrishnan and P. C. M. Planken, "Percolation-enhanced generation of terahertz pulses by optical rectification on ultrathin gold films," *Opt. Lett.*, vol. 36, no. 13, pp. 2572–2574, 2011.

[14] D. K. Polyushkin, E. Hendry, E. K. Stone, and W. L. Barnes, "THz generation from plasmonic nanoparticle arrays," *Nano Lett.*, vol. 11, no. 11, pp. 4718–4724, 2011.

[15] F. Kadlec, P. Kuzel, and J. L. Coutaz, "Study of terahertz radiation generated by optical rectification on thin gold films," *Opt. Lett.*, vol. 30, no. 11, pp. 1402–1404, 2005.

[16] F. Garwe, A. Schmidt, G. Zieger, T. May, K. Wynne, U. Hubner, M. Zeisberger, W. Paa, H. Stafast, and H. G. Meyer, "Bi-directional terahertz emission from gold-coated nanogratings by excitation via femtosecond laser pulses," *Appl. Phys. B-Lasers Opt.*, vol. 102, no. 3, pp. 551–554, 2011.

[17] A. Schmidt, F. Garwe, U. Hübner, T. May, W. Paa, M. Zeisberger, G. Zieger, and H. Stafast, "Experimental characterization of bi-directional terahertz emission from gold-coated nanogratings," *Appl. Phys. B*, vol. 109, no. 4, pp. 631–642, Nov. 2012.

[18] J. Shan, C. Weiss, R. Wallenstein, R. Beigang, and T. F. Heinz, "Origin of magnetic field enhancement in the generation of terahertz radiation from semiconductor surfaces," *Opt. Lett.*, vol. 26, no. 11, pp. 849–51, Jun. 2001.

[19] L. Myers, R. Eckardt, M. Fejer, R. Byer, W. Bosenberg, and J. Pierce, "Quasi-phase-matched optical parametric oscillators in bulk periodically poled LiNbO3," *JOSA B*, vol. 12, no. 11, pp. 2102–2116, 1995.